Version auteur de l'article : Hasnaa Meliani, Mohamed Assoul, Michael Fontaine, Vahan Malkhasyan, Alexandre Gilbin, and Guy Monteil, Femtosecond laser–matter interaction of tungsten carbide, Applied Optics, Vol. 60, Issue 3, pp. 621-625 (2021) • https://doi.org/10.1364/AO.409163

Femtosecond laser-matter interaction of tungsten carbide

HASNAA MELIANI*, MOHAMED ASSOUL, MICHAEL FONTAINE, VAHAN MALKHASYAN, ALEXANDRE GILBIN, GUY MONTEIL

University Bourgogne Franche-Comté, FEMTO-ST Institute, UMR CNRS 6174, ENSMM/UFC/UTBM, Applied Mechanics Dept., 24 chemin de l'Epitaphe, 25000, Besançon, France
**Corresponding author: hasnaa.meliani@femto-st.fr*

The purpose of this research is to investigate the femtosecond laser-matter interaction for a tungsten carbide with 10% of cobalt. A femtosecond laser (1030 nm) with a pulse duration of 400 fs have been used for this study. For cumulated fluences between 1.4 and 4 J/cm², Laser-Induced Periodic Surface Structures (LIPSS) could be produced with a low ablation rate. LIPSS had a spatial period of 665 nm and an amplitude of 225 nm. The a-thermal ablation threshold fluence have been found to be from 0.35 to 11 J/cm² in cumulated fluence for a range between 1 to 100 pulses. Thus dimples could be fabricated without any thermal effects. In addition, incubation coefficient and optical penetration depth of tungsten carbide were determined. They are equal to 0.79 and 19 nm respectively.

1. INTRODUCTION

For the last two decades, ultrashort pulsed lasers have been beneficial to handle issues in many applications from manufacturing, military, aerospace and medical industries. Nowadays, this technique is more and more employed to tune the surface properties of a material such as wettability and tribological behavior [1]. In this work, we used laser surface structuring for improving cutting results on tungsten carbide workpieces for turning applications. The desired scope is to decrease both abrasive wear and adhesion on workpieces while machining stainless steel or aluminum alloy. Nevertheless, the interaction of laser pulses with tungsten carbide material has been tackled by only few researchers. Dumitru et al. [2-5] determined the threshold fluence for texturation regime which permits to create nanoscale structures named LIPSS or "ripples". Pfeiffer [6], Calderón Urbina [7] and Neves [8] determined the a-thermal ablation threshold fluence using respectively a femtosecond, picosecond and nanosecond-lasers. For a purpose of improving workpieces made of tungsten carbide by adapting their tribological and physicochemical properties, we need to determine precisely these threshold fluences for performing desired double-scale structures on samples. In fact, we aim to produce nano- scale structures (LIPSS), micro- scale structures and a combination of nano- and micro-scale structures on tungsten carbide workpieces. Knowing the laser-matter interaction is crucial before considering laser material micromachining process. We are proposing to investigate the behavior of tungsten carbide with 10% of cobalt under femtosecond laser pulses at variable peak fluence and number of laser pulses. We will identify the laser-matter interaction regimes for the selected material and give the mapping of fluence domains corresponding to each regime. We will also determine the incubation coefficient and optical penetration depth for tungsten carbide, parameters which are indexed only by one author in literature [7].

2. MATERIALS AND METHODS

The equipment used for laser experiments was a laser source (Tangor HP model from Amplitude Systems®, France) with an average power of 100 W, a maximum pulse energy of 500 µJ at a wavelength of 1030 nm and a variable repetition rate adjustable from one shot to 2 MHz. The minimum pulse duration is equal to 400 fs. We used a Gaussian beam which had a radius of 16.67 ± 0.5 µm measured by a beam analyzer. The studied samples were made of tungsten carbide with 10% of cobalt binder and with an average grain size of 0.7 µm. The samples were mirror-polished with diamond particles (from 9 µm down to 3 µm) and washed in an ultrasonic cleaner with ethanol for 5 min before the laser machining. The resulting surface roughness was Ra = 60 nm and Rz = 80 nm. A static matrix of impacts has been performed using different values of peak fluence (from 0.028 to 5.6 J/cm^2) and various number of pulses (from 1 to 100) at a repetition rate of 1 kHz. Dimples were examined using a scanning electron microscope (SEM-FEI Quanta™ 450 W), an atomic force microscope (AFM) and a confocal microscope (Alicona Infinite focus®). These different techniques permitted either to measure dimples depth and diameter, or to reveal the morphology of the dimples, and to observe and characterize the Laser-Induced Periodic Surface Structures (LIPSS).

3. THEORY/CALCULATION

For a Gaussian beam profile shown in Figure 1.a), the spatial variation of laser fluence can be expressed as [9]:

$$F(r) = F_0 . \exp\left(-\frac{2r^2}{\pi\omega_0^2}\right) \quad , \quad F_0 = \frac{2E}{\pi\omega_0^2} \tag{1}$$

where r is the distance from the laser beam center, F_0 is the peak fluence at the center (r = 0), ω_0 is the focused beam radius at 1/e^2 of F_0, and E is the incident laser pulse energy. In case of N static impacts, when the peak fluence F_0 is above the ablation threshold fluence $F_{th}(N)$, a dimple appears by ablation process as presented in Figure 1.b).

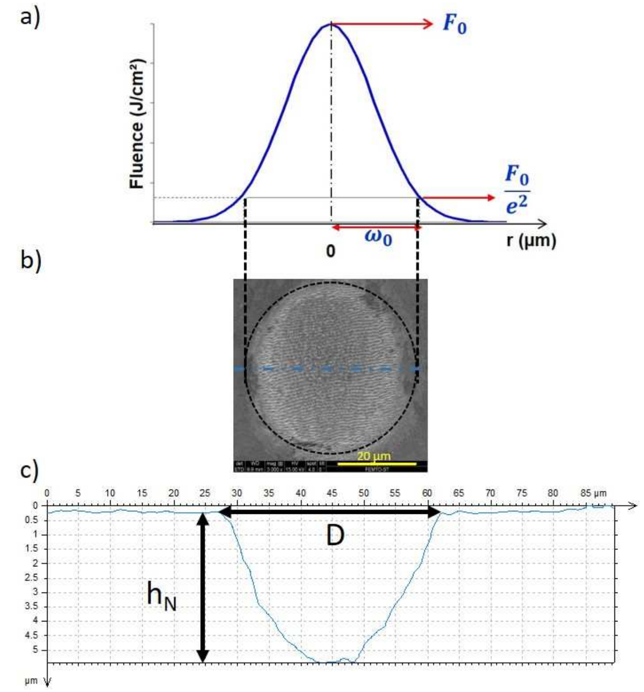

Fig. 1. a) Schematic of Gaussian beam profile, **b)** SEM image of crater generated on tungsten carbide material using a peak fluence F_0 = 2.6 J/cm^2 and N = 100 pulses, **c)** 2D profile of produced dimple (D = diameter, h_N = depth).

The diameter of ablation dimple shown in Figure 1.c) can be expressed as [9, 10]:

$$D^2 = 2\omega_0^2 \ln\left(\frac{F_0}{F_{th}(N)}\right) \tag{2}$$

where $F_{th}(N)$ is the ablation threshold fluence of N pulses. This linear dependence between D^2 and the logarithm of peak fluence permits to accurately calculate the focused beam radius ω_0 and to determine the N-pulses a-thermal ablation threshold fluence $F_{th}(N)$. This threshold fluence value is decreasing with the number of pulses as after multiple laser shots in a same area, the surface is modified and its optical properties change. An accumulation of energy occurs in the material which causes an incubation effect [11, 12]. This reaction can be expressed by the relation between the a-thermal ablation threshold fluence for N pulses $F_{th}(N)$ and the a-thermal ablation threshold fluence for 1 pulse $F_{th}(1)$ as:

$$F_{th}(N) = F_{th}(1) . N^{\xi-1} \tag{3}$$

where ξ is the response of the material to cumulative ablation shots. When ξ = 1, the threshold fluence is independent of the number of pulses and there is no incubation effect. When ξ < 1, some residual energy is left in the material between each pulse, thus decreasing the a-thermal ablation threshold fluence while increasing number of pulses.
For the a-thermal ablation regime, the ablation depth depends on the optical penetration depth α^{-1}, where α is the absorption coefficient of the material at the given laser wavelength. The ablation depth for 1-pulse is given by [13] :

$$h_1 = \alpha^{-1} . \ln\left(\frac{F_0}{F_{th}(1)}\right) \tag{4}$$

The ablation depth h_N for N pulses shown in Figure 1.c) is expressed as:

$$h_N = N . \alpha^{-1} . \ln\left(\frac{F_0}{F_{th}(N)}\right) \tag{5}$$

4. RESULTS AND DISCUSSION

As defined in Equation 2, the relationship between the measured dimple diameter squared (D^2) and the logarithm of peak fluence can be used to deduce the laser beam spot radius ω_0 and a-thermal ablation threshold fluence for N pulses. Figure 2 shows the relationship between the square of the dimple diameter and the logarithm of peak fluence for dimples produced by 10, 50 and 100 pulses at a repetition rate of 1 kHz. Applied peak fluences were calculated using measured waist size of the focused beam using Equation 1. Dimple's diameter were measured using confocal microscope (Alicona Infinite focus®). The laser beam spot radius ω_0 is calculated from the slope of the line of best fit to the data in Figure 2 for each N pulses. An average ω_0 is found to be 15.75 ± 0.8 µm µm which is close to the measured beam spot size (16.67 ± 0.5 µm). Once beam size is calculated from experimental analysis, from this point forward, applied peak fluence will be calculated using this new value of beam radius.
As the a-thermal ablation threshold fluence changes with number of pulses applied to the same spot, by an extrapolation to D^2 = 0, $F_{th}(N)$ for

each N can be determined. From Figure 2, a-thermal ablation threshold fluences were found to be 0.19 J/cm^2, 0.14 J/cm^2 and 0.11 J/cm^2 for N = 10, 50 and 100 respectively.

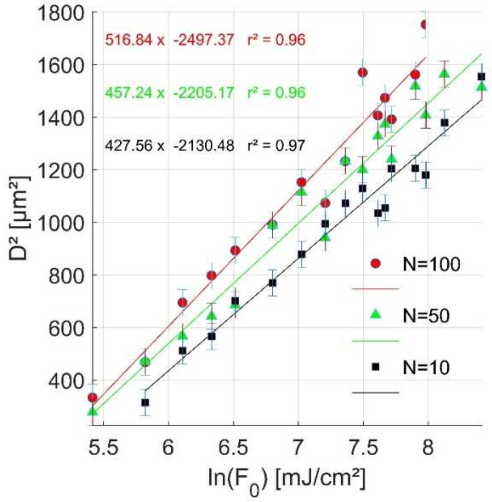

Fig. 2. Squared diameters of dimples as a function of the logarithm of laser peak fluence for N = 10, 50, 100

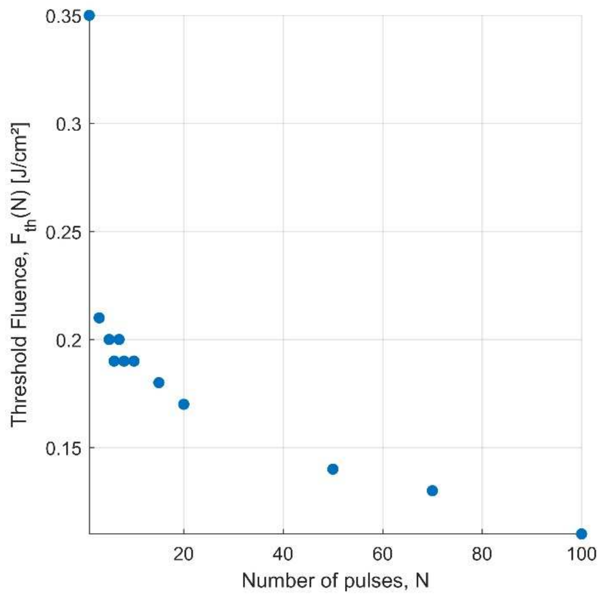

Fig. 3. Threshold fluence as a function of number of pulses.

Figure 3 shows the evolution of a-thermal ablation threshold fluence as a function of number of pulses. For a-thermal ablation regime, the range of the threshold fluence is found to be between 0.11 to 0.35 J/cm^2 from N = 100 to 1 pulses, as seen on Figure 3. It corresponds to a range of 0.35 to 11 J/cm^2 in cumulated fluence ($N \times F_0$). A-thermal ablation threshold fluence for a single-pulse is found to be $F_{th}(1)$ = 0.35 J/cm^2.

Among the few works giving results about the a-thermal ablation domain and thresholds, Neves et al. found the upper limit of the range of a-thermal ablation zone to be at 22.92 J/cm^2 in cumulated fluence starting their investigations from 3.82 J/cm^2 [8] whereas Tan et al. worked in the range between 0.49 to 4.11 J/cm^2 without defining these values as the limits of the ablation domain [14]. More complete work have been published by Dumitru et al. [4, 5], Pfeiffer [6] and Calderón Urbina [7]. Dumitru and Pfeiffer found the lower limit around 0.4 J/cm^2 and Calderón Urbina around 0.2 J/cm^2 both for a single-pulse. The variations can be explained, in one hand, by the difference of pulse duration applied, which is 10 ps for Calderón Urbina and about 100 fs for Pfeiffer and Dumitru. On the other hand, it can also be due to wavelength employed during experiments, which is 1064 nm for Calderón Urbina et al., 532 nm for Neves et al. and around 775-800 nm for the other authors. However the order of magnitude of these values are close to the measured one in the present work notwithstanding the different composition of studied materials.

Incubation coefficient ξ has been determined from slope of the line of best fit to the data in Figure 4, and found to be equal to 0.79. According to Calderón Urbina et al., the incubation coefficient for tungsten carbide is given as 0.85 for a matrix with 12% of cobalt and a grain size of 0.5 µm [7].

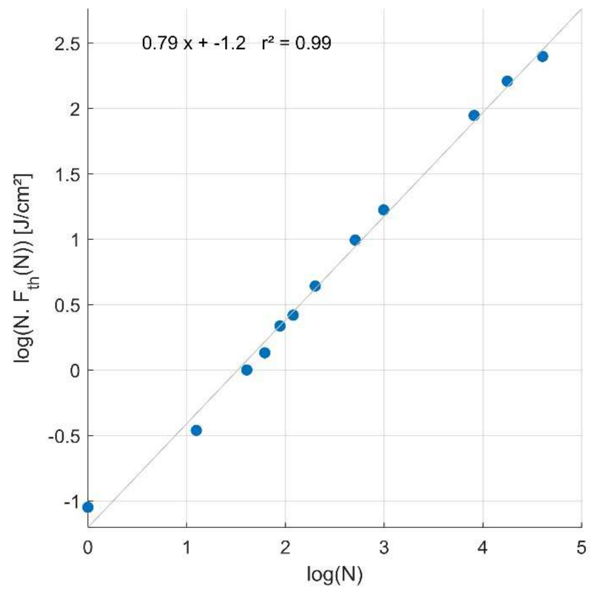

Fig. 4. Accumulation of ablation threshold versus number of pulses.

According to Equation 5, when plotting depth of ablated dimples as a function of the logarithm of peak fluence F_0 which is calculated using the new value of beam spot size (15.75 µm), as illustrated on Figure 5, optical penetration depth (α^{-1}) can be determined. Dimple's depth were measured using a confocal microscope (Alicona Infinite focus®). We found an average optical penetration depth equal to 19 ± 2.8 nm. According to Calderón Urbina and Pfeiffer, optical penetration depth for tungsten carbide is equal to 22.5 nm measured with different lasers and carbide compositions [7].

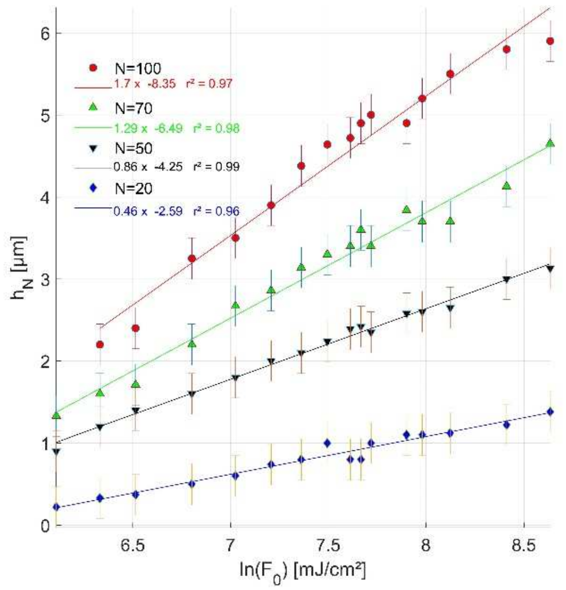

Fig. 5. Ablation depth h_N versus the logarithm of peak laser fluence for N = 20, 50, 70, 100.

Figure 6 shows the relationship between dimple depth and number of pulses for dimples produced at variable peak fluence F_0 (using ω_0 = 15.75 µm) for a fixed repetition rate of 1 kHz. There is a linear relation between ablation depth and number of pulses at different peak fluences.

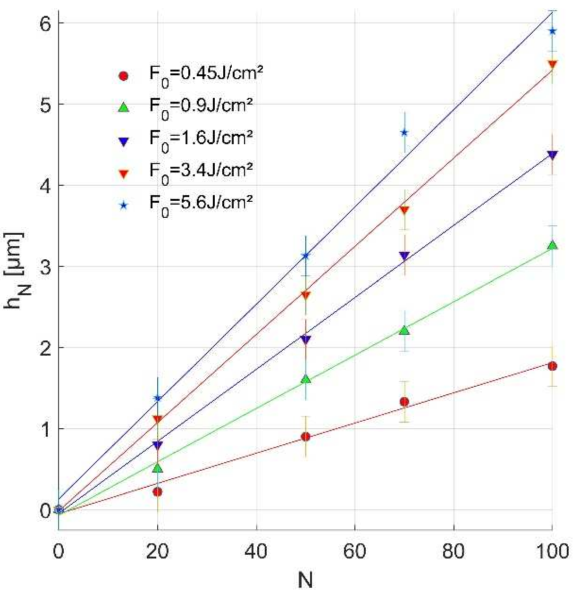

Fig. 6. Ablation depth h_N versus the number of pulses N for F_0 = 0.45, 0.9, 1.6, 3.4, 5.6 J/cm^2

No structural damage is observed on the material at peak fluences below 0.22 J/cm^2 from 1 to 100 pulses. Then, a damaged impact appears for 1-pulse at a peak fluence of 0.22 J/cm^2. So, the first interaction threshold fluence for one pulse is between 0.11-0.22 J/cm^2. According to Dumitru et al., this range is between 0.08 to 0.14 J/cm^2 for one pulse for tungsten carbide samples with 6% and 10% of cobalt binder [4, 5].

The LIPSS appear above a threshold value of fluence. Figure 7 displays LIPSS with low ablation rate produced at a peak fluence of 0.2 J/cm^2 and a number of pulses of 20. In our matrix, periodic LIPSS appeared from F_0 = 0.2 J/cm^2 for N = 7, with a mean periodicity of 665 nm and an average height of 225 nm measured using AFM technique. 2D profile of LIPSS is presented on Figure 8. These ripples had a period equal to approximately 0.6×λ_{laser}. In the literature, this kind of ripples is called coarse ripples or low spatial frequency (LSF-LIPSS) [15]. The orientation of LIPSS is perpendicular to the polarization direction of the laser beam. From AFM analysis, we could determine the range of texturation regime (LIPSS generation zone) without digging. This range is between 1.4 to 4 J/cm^2 which is a cumulated fluence (N×F_0) for a peak fluence of 0.2 J/cm^2 and a number of pulses varying from 7 to 20 pulses. For a single-pulse, threshold peak fluence of texturation regime would be between 0.22 and 0.35 J/cm^2. According to Dumitru et al., the range of texturation regime is between 0.4 to 2.8 J/cm^2 for a tungsten carbide of 10% of cobalt and a grain size of 0.5 µm [5]. Once threshold fluences for each regime were established, laser-matter interaction domain map for tungsten carbide can be drawn, as shown on Figure 9.

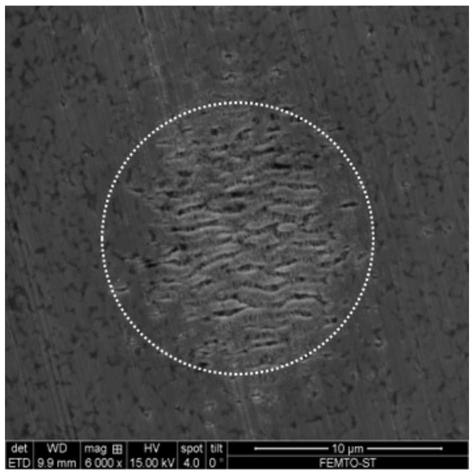

Fig. 7. SEM image of LIPSS on tungsten carbide (F_0 = 0.2 J/cm^2; N = 20).

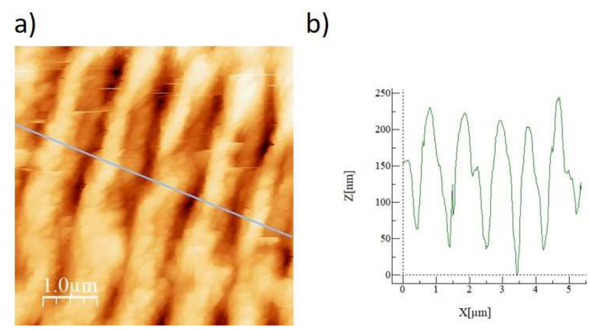

Fig. 8. Characterization of produced LIPSS using F_0 = 0.3 J/cm^2; N = 20 : **a)** AFM image 5x5 µm^2, **b)** 2D profile along LIPSS.

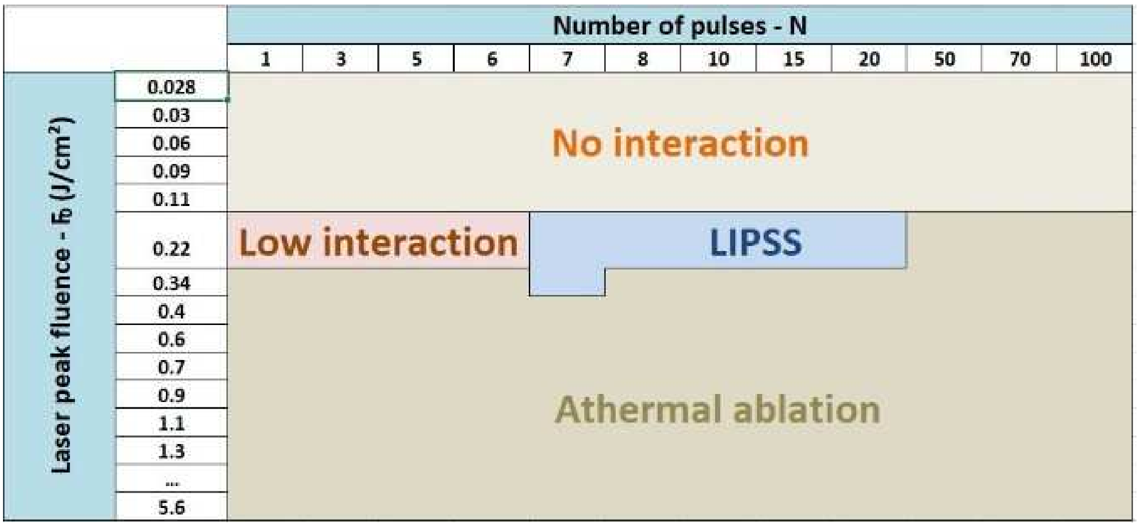

Fig. 9. Laser-matter interaction domain map for tungsten carbide.

5. CONCLUSIONS

We have investigated the laser matter-interaction for tungsten carbide with femtosecond laser for multiple number of pulses and different fluence values. The main conclusions can be summerized as follows:

(1) Three regimes were identified which correspond to: low interaction zone, LIPSS zone and a-thermal ablation zone. Figure 9 is intended to show these three range zones.
(2) Ripples could be produced starting from $N = 7$ at a peak fluence of 0.2 J/cm^2. They were perpendicular to the polarization of the laser beam and have a period equivalent to $0.6\times\lambda_{laser}$.
(3) The single pulse threshold fluence for a-thermal ablation was determined and is equal to 0.35 J/cm^2 which is close to the values of Dumitru and Pfeiffer.
(4) Incubation coefficient of tungsten carbide is found to be 0.79 in agreement with Calderón Urbina's postulated value.
(5) Optical penetration depth of tungsten carbide has been determined and found equal to 19 nm in accordance with Calderón Urbina and Pfeiffer's results using different tungsten carbide grades.
It is the first time that all the laser-matter parameters for generating ripples or femtosecond laser-matter ablation on tungsten carbide have been measured and communicated to worldwide scientific community.

Funding sources and acknowledgments. The authors gratefully acknowledged the financial support received from two industrial partners, Baron & DDLG, and by the Regional Council of Bourgogne Franche-Comté. This work was carried out within the Manufacturing 21 working group, which gathers about 20 French research laboratories. The topics covered are the modelling of the manufacturing process, virtual machining, and the emergence of new manufacturing methods.

Disclosures. The authors declare no conflicts of interest.

References

1. B.S. Yilbas and H. Ali, "Laser texturing of Hastelloy C276 alloy surface for improved hydrophobicity and friction coefficient," Optics and Lasers in Engineering, **78**, 140-147 (2016).
2. G. Dumitru, B. Lüscher, M. Krack, S. Bruneau, J. Hermann and Y. Gerbig, "Laser processing of hardmetals: Physical basics and applications," International Journal of Refractory Metals and Hard Materials, **23**, no. 4-6 SPEC. ISS., 278-286 (2005).
3. G. Dumitru, V. Romano, H.P. Weber, Y. Gerbig, H. Haefke, S. Bruneau, J. Hermann, and M. Sentis, "Femtosecond laser ablation of cemented carbides: Properties and tribological applications," Applied Physics A: Materials Science and Processing, **79**, no. 3, 629-632 (2004).
4. G. Dumitru, V. Romano, H.P. Weber, M. Sentis, and W. Marine, "Femtosecond ablation of ultrahard materials," Applied Physics A: Materials Science and Processing, **74**, no. 6, 729-739 (2002).
5. G. Dumitru, V. Romano, H.P. Weber, M. Sentis, and W. Marine, "Ablation of carbide materials with femtosecond pulses," Applied Surface Science, **205**, no. 1-4, 80-85 (2003).
6. M. Pfeiffer, A. Engel, S. Weiβmantel, S. Scholze, and G. Reisse, "Microstructuring of steel and hard metal using femtosecond laser pulses," Physics Procedia, **12**, no. PART 2, 60-66 (2011).
7. J.P. Calderon Urbina, C. Daniel, and C. Emmelmann, "Experimental and analytical investigation of cemented tungsten carbide ultrashort pulse laser ablation," Physics Procedia, **41**, 752-758 (2013).
8. D. Neves, "The laser texturing of cemented carbide surfaces," Proceedings of COBEM 2011.
9. D. Nieto, J. Arines, G. M. O'Connor and M. T. Flores-Arias, "Single-pulse laser ablation threshold of borosilicate, fused silica, sapphire, and soda-lime glass for pulse widths of 500 fs, 10 ps, 20 ns," Applied Optics, **54**, no. 29, 8596-8601 (2015).
10. P. Das Gupta and G. M. O'Connor, "Comparison of ablation mechanisms at low fluence for ultrashort and short-pulse laser exposure of very thin molybdenum films on glass," Applied Optics, **55**, no. 9, 2117-2125 (2016).
11. Y. Jee, M.F. Becker, and R. M. Walser, "Laser-induced damage on single-crystal metal surfaces," Journal of the Optical Society of America B, **5**, no. 3, 648 (1988).
12. J.I. Ahuir-Torres, M.A. Arenas, W. Perrie, and J. de Damborenea, "Influence of laser parameters in surface texturing of Ti6Al4V and AA2024-T3 alloys," Optics and lasers in Engineering, **103,** no. 3, 100-109 (2018).
13. S. Mishra and V. Yadava, "Laser Beam MicroMachining (LBMM) - A review," Optics and Lasers in Engineering, **73**, 89-122 (2015).

14. J. Tan, D. Butler, L. Sim and A. Jarfors, "Effects of laser ablation on cemented tungsten carbide surface quality," Applied Physics A: Materials Science and Processing, **101**, 265-269 (2010).
15. K.M. Tanvir Ahmmed, C. Grambow, and A.M. Kietzig, "Fabrication of Micro/Nano Structures on Metals by Femtosecond Laser Micromachining," Micromachines, **5**, 1219-1253 (2014).